








RESEARCH ARTICLE | JULY 09 2024

## Dry and wet etching of single-crystal AlN

Special Collection: [Commemorating the Career of Gerry Lučovský](#)

Hsiao-Hsuan Wan  ; Chao-Ching Chiang  ; Jian-Sian Li  ; Nahid Sultan Al-Mamun  ; Aman Haque  ;  
Fan Ren  ; Stephen J. Pearton 



*J. Vac. Sci. Technol. A* 42, 052601 (2024)

<https://doi.org/10.1116/6.0003744>



**HIDEN**  
ANALYTICAL

## Instruments for Advanced Science

- Knowledge
- Experience ■ Expertise

[Click to view our product catalogue](#)

Contact Hiden Analytical for further details:

[www.HidenAnalytical.com](http://www.HidenAnalytical.com)  
[info@hiden.co.uk](mailto:info@hiden.co.uk)

### Gas Analysis

- ▶ dynamic measurement of reaction gas streams
- ▶ catalysis and thermal analysis
- ▶ molecular beam studies
- ▶ dissolved species probes
- ▶ fermentation, environmental and ecological studies

### Surface Science

- ▶ UHV TPD
- ▶ SIMS
- ▶ end point detection in ion beam etch
- ▶ elemental imaging - surface mapping

### Plasma Diagnostics

- ▶ plasma source characterization
- ▶ etch and deposition process reaction kinetic studies
- ▶ analysis of neutral and radical species

### Vacuum Analysis

- ▶ partial pressure measurement and control of process gases
- ▶ reactive sputter process control
- ▶ vacuum diagnostics
- ▶ vacuum coating process monitoring

# Dry and wet etching of single-crystal AlN

Cite as: J. Vac. Sci. Technol. A 42, 052601 (2024); doi: 10.1116/6.0003744

Submitted: 7 May 2024 · Accepted: 17 June 2024 ·

Published Online: 9 July 2024



Hsiao-Hsuan Wan,<sup>1,a)</sup>  Chao-Ching Chiang,<sup>1</sup>  Jian-Sian Li,<sup>1</sup>  Nahid Sultan Al-Mamun,<sup>2</sup>  Aman Haque,<sup>2</sup>   
Fan Ren,<sup>1</sup>  and Stephen J. Pearton<sup>3</sup> 

## AFFILIATIONS

<sup>1</sup>Department of Chemical Engineering, University of Florida, Gainesville, Florida 32611

<sup>2</sup>Department of Mechanical Engineering, The Pennsylvania State University, University Park, Pennsylvania 16802

<sup>3</sup>Department of Materials Science and Engineering, University of Florida, Gainesville, Florida 32611

**Note:** This paper is part of the Special Topic Collection Commemorating the Career of Gerry Lucovsky.

**a) Electronic mail:** [hwan@ufl.edu](mailto:hwan@ufl.edu)

## ABSTRACT

The dry etching of high crystal quality *c*-plane AlN grown by metal organic chemical vapor deposition was examined as a function of source and chuck power in inductively coupled plasmas of Cl<sub>2</sub>/Ar or Cl<sub>2</sub>/Ar/CHF<sub>3</sub>. Maximum etch rates of ~1500 Å min<sup>-1</sup> were obtained at high powers, with selectivity over SiO<sub>2</sub> up to 3. The as-etched surfaces in Cl<sub>2</sub>/Ar/CHF<sub>3</sub> have F-related residues, which can be removed in NH<sub>4</sub>OH solutions. The Al-polar basal plane was found to etch slowly in either KOH or H<sub>3</sub>PO<sub>4</sub> liquid formulations with extensive formation of hexagonal etch pits related to dislocations. The activation energies for KOH- or H<sub>3</sub>PO<sub>4</sub>-based wet etching rates within these pits were 124 and 183 kJ/mol, respectively, which are indicative of reaction-limited etching.

Published under an exclusive license by the AVS. <https://doi.org/10.1116/6.0003744>

## I. INTRODUCTION

Aluminum nitride (AlN) possesses a bandgap energy of 6.28 eV and can be grown in high-quality bulk crystals with diameters of up to 4 in., accompanied by a high breakdown field of approximately 15 MV cm<sup>-1</sup>.<sup>1–8</sup> These intrinsic characteristics position AlN as a promising candidate for various applications in military and civilian power and extreme environment electronics, including high-temperature, high-radiation exposure, DC microgrids, pulsed power weaponry, and systems operating under extreme conditions, alongside switching and transmission within high-voltage direct current (HV-DC) power grids.<sup>1,2,8–12</sup> AlN demonstrates superior performance at elevated temperatures and powers compared to narrower bandgap semiconductors. In power switching applications, such Ultra-wide Band Gap (UWBG) semiconductors exhibit diminished resistive energy losses, potentially replacing complex stacked configurations with single devices.<sup>2,5,6,8</sup> Moreover, in radiofrequency applications, they facilitate the development of more potent radar systems with extended ranges and hold promise for employment in directed energy systems.<sup>1,2,8</sup> Current research efforts focus on control of doping and achieving thick (>10 μm) lightly doped epitaxial structures for vertical power rectifiers.<sup>4,7,9,11,13–16</sup> To fully harness the material's advantages, advancements in bulk and epitaxial

crystal growth, low-resistance Ohmic contacts,<sup>17</sup> controlled etching,<sup>18,19</sup> more efficient doping methodologies,<sup>20,21</sup> suitable dielectrics with appropriate band offsets to AlN,<sup>22</sup> and minimization of damage during pattern transfer processes are imperative.<sup>13,18,23–46</sup> For example, one drawback is the low conductivity of doped layers exacerbated by the fact AlN has a large carrier effective mass ( $m_e^* = 0.33 m_e$  and heavy hole  $m_h^* = 3.5 m_h$ ).<sup>4</sup>

Historically, AlN is primarily considered to be an insulator; however, recent breakthroughs in achieving high *n*-type and *p*-type doping levels have revitalized interest in this material for vertical device applications and commercialization of power electronics.<sup>4,5,7,9,11,15</sup> There are a number of critical processing steps that need development for this to occur. For example, the patterning of AlN is difficult because of its strong atomic bonding and relative chemical inertness, leading to low etch rates for both wet and dry etching.<sup>18,23,25–40,42,44,45,47</sup> However, a feature of previous work has been that improving materials quality as epitaxial growth processes are optimized, leads to even lower etch rates.<sup>32,34,38</sup> Dry etching is typically performed in Cl<sub>2</sub>-based plasmas,<sup>23,25–31</sup> while for wet etching, KOH, hot H<sub>3</sub>PO<sub>4</sub>, or tetra methyl ammonium hydroxide (TMAH) above 80 °C have been employed.<sup>18,19,32–36,38</sup> There are few reports that address the behavior of planar AlN substrates in alkaline and acidic solutions. Given the resurgence of interest in AlN for

04 September 2024 19:09:17

power electronic devices and photonic arrays, in this paper, we revisited plasma and wet chemical etching of this material.

## II. EXPERIMENTAL

The initial AlN-based substrates comprised  $2.7\ \mu\text{m}$  of c-plane, Al-polar AlN fabricated via metal organic chemical vapor deposition (MOCVD) atop 270 nm AlN buffer layers synthesized through hydride vapor epitaxy (HVE) on sapphire substrates. This is important to note since this is the commonly used polarity and reports demonstrate that N-polar AlN etches at much higher rates than c-plane,<sup>35</sup> along with non-polar, a-plane orientations. Previous results have shown x-ray rocking curve full width at half maxima for peaks at  $14.2^\circ$  and  $17.75^\circ$  for the (0 0 0 2) and (20 $\bar{2}$ 4) planes of 175 and 192 arcsec, respectively.<sup>43</sup> A cross-sectional TEM image of the epilayer is shown in Fig. 1.

Dry etching was conducted utilizing a Unaxis Shuttlelock reactive ion etcher with inductively coupled plasma module under the following conditions: discharges of 15 standard cubic centimeters per minute (SCCM) of  $\text{Cl}_2$  and 5 SCCM of Ar, sometimes supplemented with 5 SCCM  $\text{CHF}_3$ , maintained at a constant pressure of 5 mTorr. The ICP source power and RF chuck power were systematically adjusted to modulate plasma density and ion energy, respectively, thereby affecting etch rates. The etching was performed at  $15^\circ\text{C}$ , with the samples affixed to a water-cooled platen using thermal grease. Given the brief duration of the etching process, significant temperature elevation was not anticipated, and there was no observed evidence of thermal degradation of the resist masks. Etch rates were determined by evaluating the etch depth post-removal of the photoresist, employing a Tencor profilometer. Importantly, short plasma exposures lasting approximately 1–2 min did not lead to notable surface roughening. The samples were lithographically patterned using PR-1818 photoresist with a thickness of approximately  $1\text{--}2\ \mu\text{m}$ . All etching procedures were conducted at  $15^\circ\text{C}$ , with an

etch time of 2 min. Subsequently, the etch depth and surface root mean square (RMS) roughness of the processed samples were assessed utilizing a surface profilometer (Tencor alpha-step IQ).

Wet etching was performed in KOH or  $\text{H}_3\text{PO}_4$  solutions from 25 to  $100^\circ\text{C}$  using Ti/Au and  $\text{SiO}_2$  masking, respectively. Surface profilometry was used to measure the vertical and lateral etch rates, the latter around the etch pits that formed on the surface. We employed a wagon wheel structure, pioneered by Wind and Hines,<sup>44</sup> to attempt to measure the nonpolar etch rates. This structure uses the geometric amplification of the direction-dependent etches, inherent to the etching of wedge-shaped structures.

To prevent surface contamination, the specimens underwent x-ray photoelectron spectroscopy (XPS) analyses under controlled atmospheric conditions, excluding prior exposure to ambient air.<sup>43</sup> For the determination of valence band offsets, preliminary XPS survey scans were conducted to characterize the surface chemical composition of NiO,  $\text{SiO}_2$ , ITO, and AlN, facilitating subsequent high-resolution investigations for chemical state identification. The XPS analysis was performed utilizing a Ulvac PHI Versaprobe II system equipped with a monochromatic aluminum x-ray source emitting at 1486.6 eV, operating at a power setting of  $100\ \mu\text{m}$ , 25 W, and 15 kV.<sup>43</sup> The scanning x-ray microprobe covered an analysis area of  $100 \times 100\ \mu\text{m}^2$ , employing a take-off angle of  $45^\circ$  and an acceptance angle of  $\pm 7$  degrees. High-resolution scans utilized an electron pass energy of 23.5 eV, whereas survey scans employed a pass energy of 187.5 eV. The estimated escape depth of electrons was approximately 80 Å.

To compensate for charge effects during XPS measurements, an electron flood gun and low-energy ion gun combination were employed, necessitated by the dielectric properties of the films under study. Nevertheless, complete neutralization of surface charge was not consistently achieved with the flood gun alone, mandating supplementary corrections. Charge correction was facilitated by referencing the known position of the adventitious carbon (C–C) line in the C 1s spectra at 284.8 eV.

04 September 2024 19:09:17

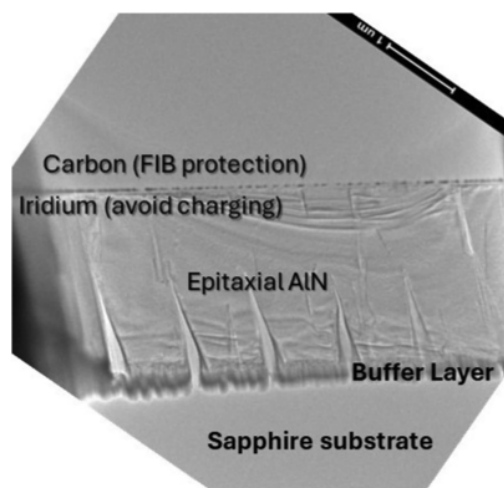


**FIG. 1.** Cross-section TEM image of a  $2.7\ \mu\text{m}$  thick AlN layer grown on a low temperature buffer on a sapphire substrate.

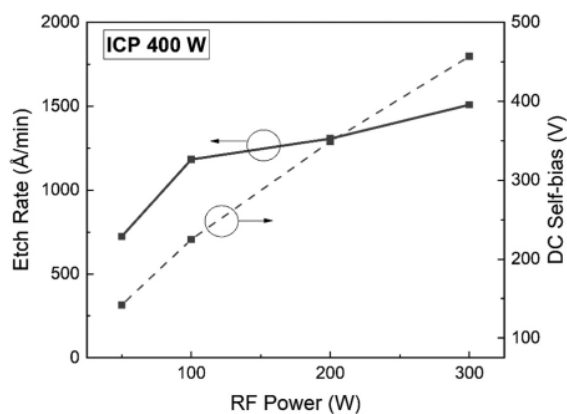


**FIG. 2.** Dry etch rate of AlN in 15  $\text{Cl}_2/5$  Ar discharges with a fixed ICP source power of 400 W, as a function of RF chuck power. The corresponding dc self-biases are also shown.

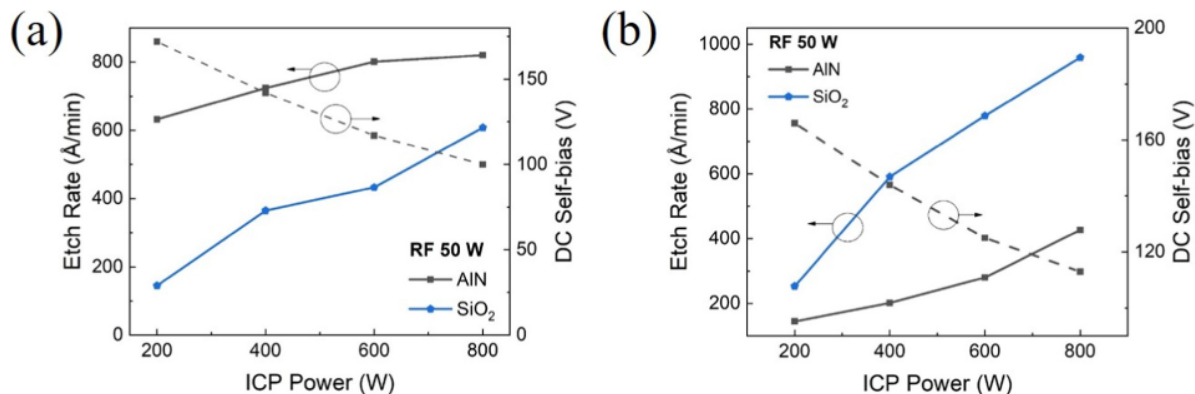


**FIG. 3.** Dry etch rate of AlN and SiO<sub>2</sub> in (a) 15 Cl<sub>2</sub>/5 Ar or (b) 15 Cl<sub>2</sub>/5 Ar/5 CHF<sub>3</sub> discharges with a fixed RF source power of 50 W, as a function of ICP source power. The corresponding dc self-biases are also shown.

### III. RESULTS AND DISCUSSION

#### A. Dry etching

Figure 2 shows the dry etch rate of AlN in 15 Cl<sub>2</sub>/5 Ar discharges with a fixed ICP source power of 400 W, as a function of RF chuck power. The corresponding dc self-biases are also shown. These are closely related to the incident ion energies, since these are the voltages that accelerate the ions across the plasma sheath to the sample electrode.<sup>25</sup> DC self-bias is the voltage that develops on the surface of the powered electrode in the plasma sheath due to the difference in mobility between electrons and ions. This bias voltage arises because electrons, being much lighter, respond more quickly to the electric field than ions, creating a net negative charge on the electrode surface relative to the plasma.<sup>25</sup> The maximum etch rate obtained is ~1500 Å min<sup>-1</sup>, which is slower than reported for

sputtered AlN or materials grown in the early days by the main epitaxial techniques. At low RF powers, the etch rate increases almost linearly with dc self-bias, indicating that bond-breaking and subsequent desorption of the etch products are rate-limiting. At higher powers, the etch rate begins to saturate and may be reactant limited, although we cannot exclude ion flux saturation. At lower RF powers, increasing the power can lead to a proportional increase in the number of ions bombarding the substrate surface. However, at higher RF powers, the number of ions may reach a saturation point where further increases in RF power do not significantly increase the ion flux. This saturation occurs because the plasma becomes

04 September 2024 19:09:17

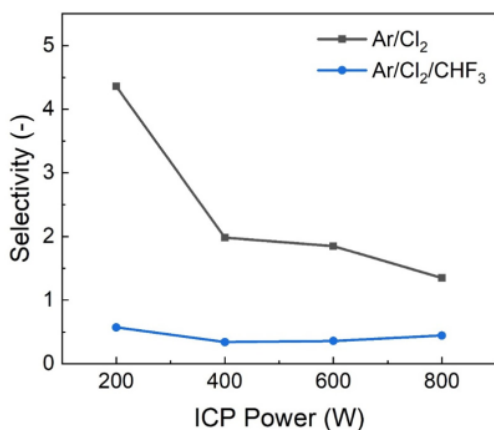


**FIG. 4.** Selectivity for dry etching of SiO<sub>2</sub> over AlN as a function of ICP power at a fixed RF power of 50 W.

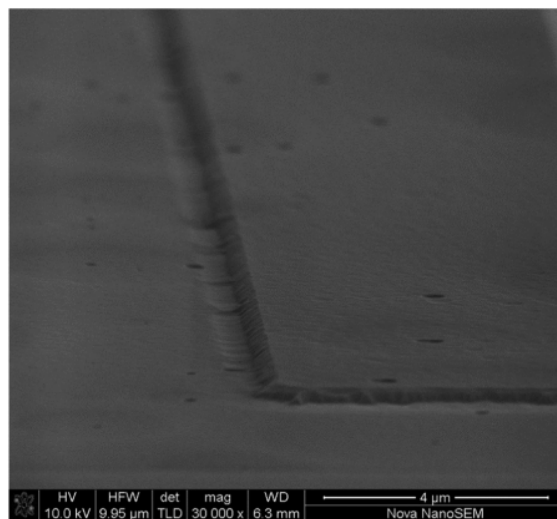


**FIG. 5.** SEM image of feature etched into AlN using a 15 Cl<sub>2</sub>/5 Ar plasma with RF power of 300 W and ICP power of 400 W. The initial photoresist mask has been removed.

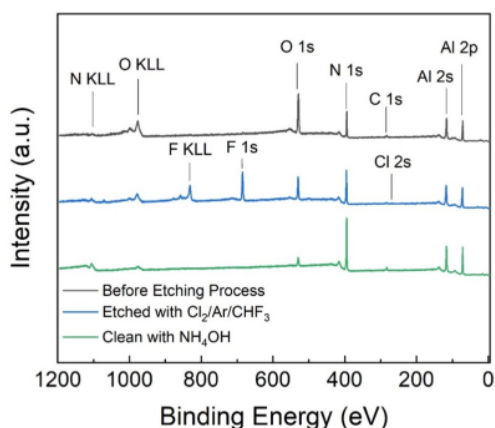


**FIG. 6.** Survey XPS spectra from AlN after exposure to the Cl<sub>2</sub>/Ar/CHF<sub>3</sub> discharge and then subsequent cleaning in NH<sub>4</sub>OH.

more collisional at higher powers, leading to reduced ion mobility and increased recombination, thereby limiting the number of ions available for etching.<sup>26</sup>

The etch rate decreased when CHF<sub>3</sub> was added to the plasma chemistry, as shown in Fig. 3, which displays the dry etch rate of AlN and SiO<sub>2</sub> in (a) 15 Cl<sub>2</sub>/5 Ar or (b) 15 Cl<sub>2</sub>/5 Ar/5 CHF<sub>3</sub> discharges with a fixed RF source power of 50 W, as a function of ICP source power. The AlN etch rate roughly decreases by a factor of 2 when CHF<sub>3</sub> is added, since the volatility of AlF<sub>3</sub> is very low and its formation is used as an etch stop reaction.<sup>23,25</sup> It also increases the etch rate of SiO<sub>2</sub>, leading to a decrease in etch selectivity for AlN over SiO<sub>2</sub>. This is shown in Fig. 4, which displays selectivity for dry etching of SiO<sub>2</sub> over AlN as a function of ICP power at a fixed RF power of 50 W. Figure 5 shows an SEM image of a feature etched into AlN using a 15 Cl<sub>2</sub>/5 Ar plasma with an RF power of 300 W and an ICP power of 400 W. The initial photoresist mask has been removed. The field region has similar surface roughness to the initially masked area.

Figure 6 shows survey XPS spectra from AlN after exposure to the Cl<sub>2</sub>/Ar/CHF<sub>3</sub> discharge and then subsequent cleaning in

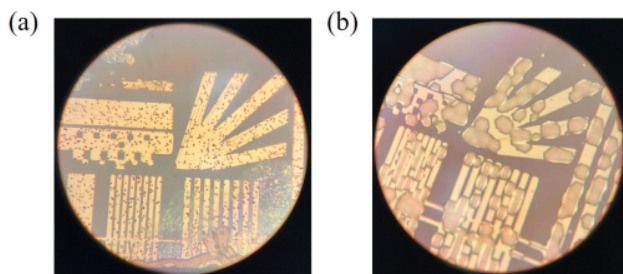


**FIG. 7.** Optical images of the masked and etched surface of AlN samples in H<sub>3</sub>PO<sub>4</sub> (a) at 60 °C for 15 min or (b) 80 °C for 8 min.

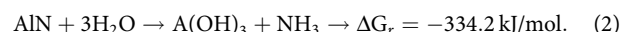
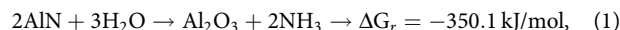
NH<sub>4</sub>OH. AlCl<sub>3</sub> has higher volatility than AlF<sub>3</sub>, so it is less present on the surface. This explains why the F peak is more obvious in the XPS spectra compared to the Cl peak, and also the etch rate becomes lower when we added CHF<sub>3</sub>. After rinsing in NH<sub>4</sub>OH, the F signal is removed below the detection limit of the XPS system.

## B. Wet etching

Hexagonal pits, similar to those reported previously, were observed after wet etching of the Al-polar surfaces.<sup>19,33,40,41,43</sup> These result from screw dislocations within the material that terminate at the surface and are preferentially etched relative to defect-free areas.<sup>40,41</sup> AlN etches in KOH via the formation and dissolution of oxides and hydroxides. From energy calculations, the negative Gibbs free energy for AlN products points to a favorable reaction, where the aluminum oxides and hydroxides are much more able to dissolve rapidly in solution. For phosphoric acid etching however, Reiner *et al.*<sup>41</sup> postulated a three-step process, where phosphoric acid is actually a reaction partner during the etch, rather than a catalyst, as seen in KOH. So, initially, the phosphoric acid dissociates in solution and the phosphate group attaches to the metal atom. Subsequently, the bonds rearrange to free up the atom, with dissolution of the Al-phosphate complex (AlH<sub>2</sub>PO<sub>4</sub><sup>2+</sup>).<sup>41</sup> The etch pits eventually come to dominate the surface of the etched regions, as shown in the optical microscope images of Fig. 7, displaying the masked and etched surface of AlN samples in H<sub>3</sub>PO<sub>4</sub> (a) at 60 °C for 15 min or (b) 80 °C for 8 min. Magnified views of the pits and the morphology within these pits are shown in Fig. 8(a), which display SEM images of the pits formed on the surface of AlN after etching in KOH at 80 °C. Figure 8(b) shows magnified views of a large deep pit and Fig. 8(c) shows the shallow, smaller pits. Figure 9 shows SEM images of the bottom of one of the larger pits, showing the exposed buffer layer and the small hexagonal pits formed in that with the sapphire underneath. The sidewall of the etched large pit is shown in more detail in the images.

The activation energy of the etching of c-plane AlN within the large hexagonal pits in 15% KOH was 124 kJ/mol (or 5.38 eV) as shown in Fig. 10. This is indicative of a reaction rate based etch. By contrast, characteristics of diffusion-limited etching include a square root dependence of etch depth on etch time, an activation energy ≤ 6 kcal mol<sup>-1</sup> and a strong dependence of etch rate on solution agitation.<sup>32</sup> Our results did not show any of these characteristics. Note that there was no appreciable etching until >50 °C.

The etch rate of AlN with 85% H<sub>3</sub>PO<sub>4</sub> at various temperatures is shown in Fig. 11 on (a) linear scale and (b) log scale. The activation energy is 183 kJ/mol (7.94 eV), also characteristic of reaction-limited etching. The likely etch reactions are shown below,



The Gibbs free energies of these reactions indicate that the formation of aluminum-based oxides and hydroxides are favorable during the etch process.<sup>46</sup>

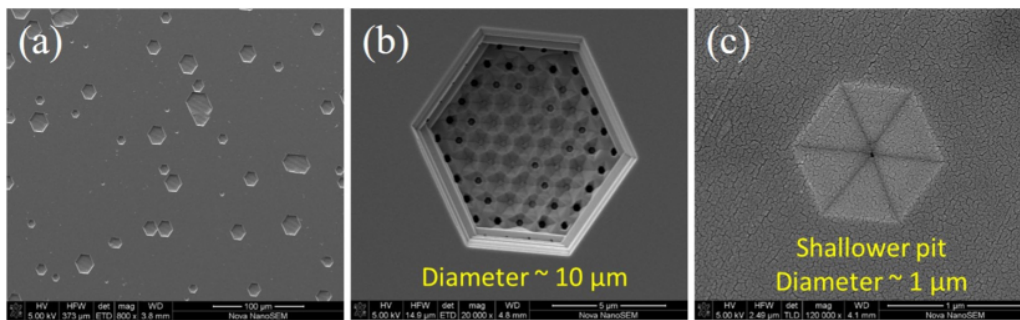


**FIG. 8.** SEM images of the AlN surface after etching in KOH at 80 °C. (a) Pits formed on the surface (b) Magnified view of large deep pit and (c) shallow, smaller pits.

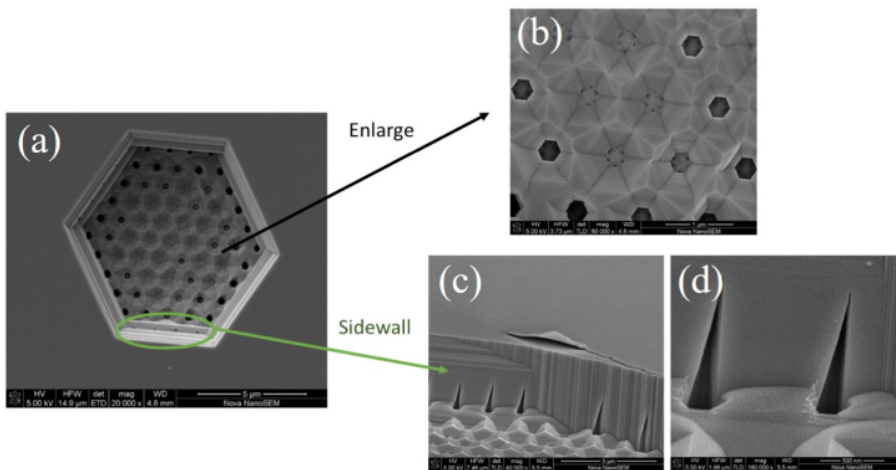


**FIG. 9.** SEM images of the bottom of one of the larger pits, showing (a) the exposed buffer layer, (b) the small hexagonal pits formed in that with the sapphire underneath, and (c) and (d) the more detailed images of the sidewall of the etched large pit.

04 September 2024 19:09:17

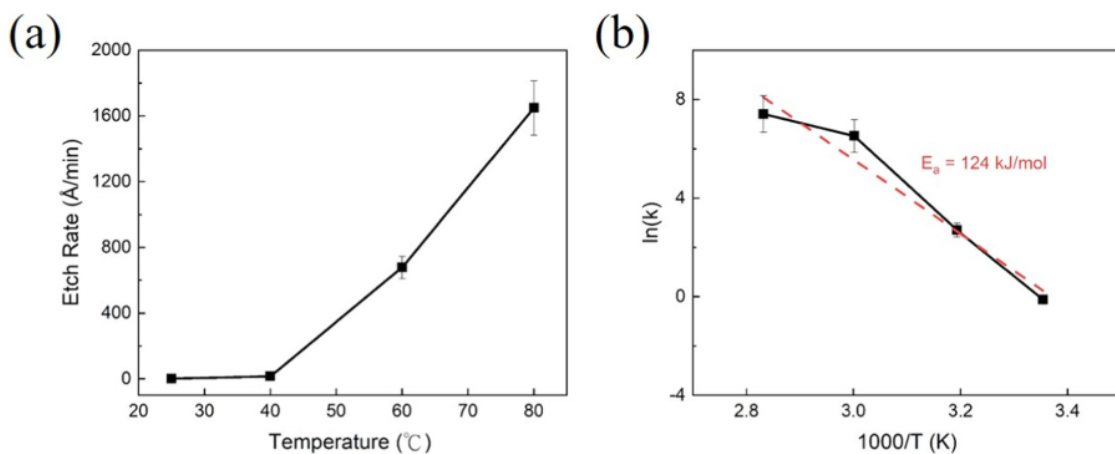


**FIG. 10.** Etch rate of AlN with 15% KOH at various temperatures in (a) a linear scale and (b) a log scale. The activation energy is 124 kJ/mol.

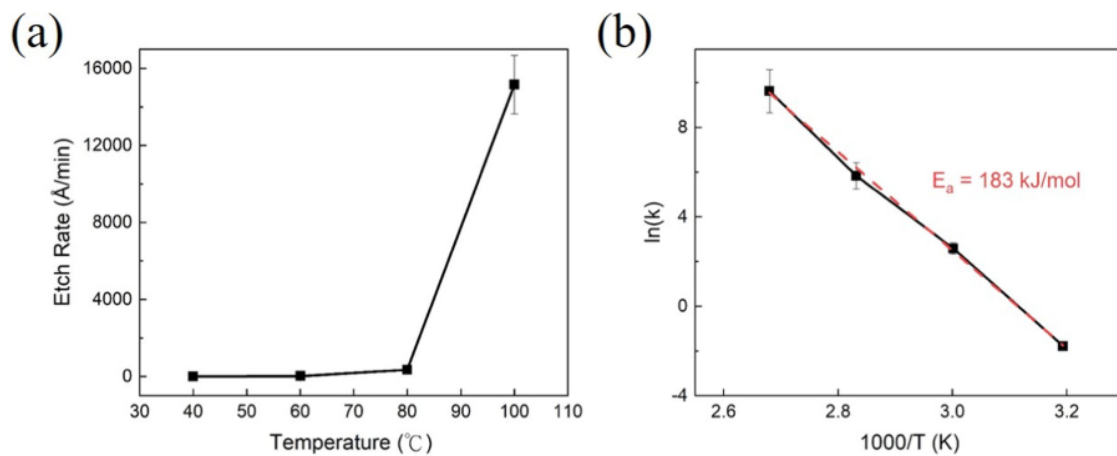


**FIG. 11.** Etch rate of AlN with 85%  $\text{H}_3\text{PO}_4$  at various temperatures in (a) a linear scale and (b) a log scale. The activation energy is 183 kJ/mol.

#### IV. SUMMARY AND CONCLUSIONS

Dry etching of high quality AlN was examined in  $\text{Cl}_2$ -based ICP discharges. Practical etch rates above  $1000 \text{ \AA min}^{-1}$  were achieved at moderate RF powers ( $>100 \text{ W}$ ) and source powers (400 W). Residues from the etch products could be removed by standard chemical cleaning. The vertical etch rate of AlN in wet etch solutions was negligibly small under most conditions. However, hexagonal pits were formed at much faster etch rates on Al polar AlN (0 0 0 1) crystals after etching in KOH or  $\text{H}_3\text{PO}_4$ . These etch pits had a hexagonal inverse pyramid shape surrounded by six  $\{10\bar{1}1\}$  planes. The activation energies of etching indicated a reaction-limited mechanism.

#### ACKNOWLEDGMENTS

The work was performed as part of Interaction of Ionizing Radiation with Matter University Research Alliance (IIRM-URA), sponsored by the Department of the Defense, Defense Threat Reduction Agency under Award No. HDTRA1-20-2-0002. The content of the information does not necessarily reflect the position or the policy of the federal government, and no official endorsement should be inferred. A.H. also acknowledges support from the U.S. National Science Foundation (ECCS No. 2015795).

#### AUTHOR DECLARATIONS

##### Conflict of Interest

The authors have no conflicts to disclose.

##### Author Contributions

**Hsiao-Hsuan Wan:** Conceptualization (equal); Formal analysis (equal); Methodology (equal); Writing – review & editing (equal).  
**Chao-Ching Chiang:** Conceptualization (equal); Formal analysis (equal); Methodology (equal); Writing – review & editing (equal).  
**Jian-Sian Li:** Conceptualization (equal); Formal analysis (equal);

Methodology (equal); Writing – review & editing (equal). **Nahid Sultan Al-Mamun:** Formal analysis (equal); Writing – review & editing (equal). **Aman Haque:** Formal analysis (equal); Writing – original draft (supporting); Writing – review & editing (equal). **Fan Ren:** Conceptualization (equal); Formal analysis (equal); Methodology (equal); Writing – review & editing (equal). **Stephen J. Pearton:** Conceptualization (equal); Formal analysis (equal); Methodology (equal); Writing – original draft (equal); Writing – review & editing (equal).

#### DATA AVAILABILITY

The data that support the findings of this study are available within the article.

#### REFERENCES

- M. H. Wong, O. Bierwagen, R. J. Kaplar, and H. Umezawa, *J. Mater. Res.* **36**, 4601 (2021).
- M. Xu, D. Wang, K. Fu, D. H. Mudiyansele, H. Fu, and Y. Zhao, *Oxford Open Mater. Sci.* **2**, itac004 (2022).
- M. E. Coltrin and R. J. Kaplar, *J. Appl. Phys.* **121**, 055706 (2017).
- W. A. Doolittle *et al.*, *Appl. Phys. Lett.* **123**, 070501 (2023).
- A. L. Hickman, R. Chaudhuri, S. J. Bader, K. Nomoto, L. Li, J. C. Hwang, H. G. Xing, and D. Jena, *Semicond. Sci. Tech.* **36**, 044001 (2021).
- M. Hiroki, Y. Taniyasu, and K. Kumakura, *IEEE Electr. Device Lett.* **43**, 350 (2022).
- M. I. Khan, C. Lee, and E. Ahmadi, *Appl. Phys. Lett.* **124**, 062107 (2024).
- J. Tsao *et al.*, *Adv. Electron. Mater.* **4**, 1600501 (2018).
- H. Ahmad, Z. Engel, C. M. Matthews, S. Lee, and W. A. Doolittle, *J. Appl. Phys.* **131**, 175701 (2022).
- A. G. Baca, A. M. Armstrong, A. A. Allerman, E. A. Douglas, C. A. Sanchez, M. P. King, M. E. Coltrin, T. R. Fortune, and R. J. Kaplar, *Appl. Phys. Lett.* **109**, 033509 (2016).
- J. S. Harris *et al.*, *Appl. Phys. Lett.* **112**, 152101 (2018).
- O. Slobodyan, J. Flicker, J. Dickerson, J. Shoemaker, A. Binder, T. Smith, S. Goodnick, R. Kaplar, and M. Hollis, *J. Mater. Res.* **37**, 849 (2022).
- P. Bagheri *et al.*, *J. Appl. Phys.* **132**, 185703 (2022).

- <sup>14</sup>H. M. Foronda *et al.*, *Appl. Phys. Lett.* **117**, 221101 (2020).
- <sup>15</sup>Y.-H. Liang and E. Towe, *Appl. Phys. Rev.* **5**, 011107 (2018).
- <sup>16</sup>J. L. Lyons and C. G. Van de Walle, *Phys. Status Solidi-R* **15**, 2100218 (2021).
- <sup>17</sup>E. Douglas, S. Reza, C. Sanchez, D. Koleske, A. Allerman, B. Klein, A. Armstrong, R. Kaplar, and A. Baca, *Phys. Status Solidi A* **214**, 1600842 (2017).
- <sup>18</sup>W. Guo, R. Kirste, I. Bryan, Z. Bryan, L. Hussey, P. Reddy, J. Tweedie, R. Collazo, and Z. Sitar, *Appl. Phys. Lett.* **106**, 082110 (2015).
- <sup>19</sup>B. A. Kazanowska, "Chemical wet etching of Al(x) Ga(1-x)N ( $0 \leq x \leq 1$ ) nanostructures," Dissertation (University of Florida, 2021).
- <sup>20</sup>A. Azarov *et al.*, *Nat. Commun.* **14**, 4855 (2023).
- <sup>21</sup>M. Hayden Breckenridge *et al.*, *Appl. Phys. Lett.* **116**, 172103 (2020).
- <sup>22</sup>J. Robertson, *Rep. Prog. Phys.* **69**, 327 (2005).
- <sup>23</sup>F. Khan, L. Zhou, V. Kumar, I. Adesida, and R. Okojie, *Mater. Sci. Eng.: B* **95**, 51 (2002).
- <sup>24</sup>R. Shul, S. Kilcoyne, M. Hagerott Crawford, J. Parmeter, C. Vartuli, C. Abernathy, and S. Pearton, *Appl. Phys. Lett.* **66**, 1761 (1995).
- <sup>25</sup>R. Shul *et al.*, *J. Vac. Sci. Technol. A* **16**, 1621 (1998).
- <sup>26</sup>S. Smith, C. Wolden, M. Bremser, A. Hanser, R. Davis, and W. Lampert, *Appl. Phys. Lett.* **71**, 3631 (1997).
- <sup>27</sup>C. Vartuli, J. MacKenzie, J. Lee, C. Abernathy, S. Pearton, and R. Shul, *J. Appl. Phys.* **80**, 3705 (1996).
- <sup>28</sup>C. Vartuli, S. Pearton, J. Lee, J. Hong, J. MacKenzie, C. Abernathy, and R. Shul, *Appl. Phys. Lett.* **69**, 1426 (1996).
- <sup>29</sup>K. Zhu, V. Kuryatkov, B. Borisov, J. Yun, G. Kipshidze, S. Nikishin, H. Temkin, D. Aurongzeb, and M. Holtz, *J. Appl. Phys.* **95**, 4635 (2004).
- <sup>30</sup>K. Airola, S. Mertin, J. Likonen, E. Hartikainen, K. Mizohata, J. Dekker, A. T. Sebastian, and T. Pensala, *Materialia* **22**, 101403 (2022).
- <sup>31</sup>V. Bliznetsov, B. H. B. Johari, M. T. Chentir, W. H. Li, L. Y. Wong, S. Merugu, X. L. Zhang, and N. Singh, *J. Micromech. Microeng.* **23**, 117001 (2013).
- <sup>32</sup>W. Guo, J. Xie, C. Akouala, S. Mita, A. Rice, J. Tweedie, I. Bryan, R. Collazo, and Z. Sitar, *J. Cryst. Growth* **366**, 20 (2013).
- <sup>33</sup>J. Mileham, S. Pearton, C. Abernathy, J. MacKenzie, R. Shul, and S. Kilcoyne, *Appl. Phys. Lett.* **67**, 1119 (1995).
- <sup>34</sup>P. Murali, *AlN Thin Film Processing and Basic Properties* (Springer, Cham, 2017).
- <sup>35</sup>R. M. Pinto, V. Gund, C. Calaza, K. Nagaraja, and K. Vinayakumar, *Microelectron. Eng.* **257**, 111753 (2022).
- <sup>36</sup>C. Vartuli, S. Pearton, J. Lee, C. Abernathy, J. MacKenzie, J. Zolper, R. Shul, and F. Ren, *J. Electrochem. Soc.* **143**, 3681 (1996).
- <sup>37</sup>E. Wistrela, M. Schneider, A. Bittner, and U. Schmid, *Microsyst. Technol.* **22**, 1691 (2016).
- <sup>38</sup>D. Zhuang and J. Edgar, *Mater. Sci. Eng.* **48**, 1 (2005).
- <sup>39</sup>M. Bickermann, S. Schmidt, B. Epelbaum, P. Heimann, S. Nagata, and A. Winnacker, *J. Cryst. Growth* **300**, 299 (2007).
- <sup>40</sup>D. Chen, D. Xu, J. Wang, and Y. Zhang, *J. Phys. D: Appl. Phys.* **41**, 235303 (2008).
- <sup>41</sup>Y. Choi, R. Choi, and J. Kim, *Appl. Surf. Sci.* **509**, 145279 (2020).
- <sup>42</sup>Y. Ha Choi, K. H. Baik, R. Choi, J. Oh, and J. Kim, *ECS J. Solid State Sci. Technol.* **8**, N42 (2019).
- <sup>43</sup>D. C. Hays, B. Gila, S. Pearton, and F. Ren, *Appl. Phys. Rev.* **4**, 021301 (2017).
- <sup>44</sup>M. Reiner, M. Reiss, T. Brünig, L. Knuuttila, R. Pietschnig, and C. Ostermaier, *Phys. Status Solidi B* **252**, 1121 (2015).
- <sup>45</sup>R. A. Wind and M. A. Hines, *Surf. Sci.* **460**, 21 (2000).
- <sup>46</sup>D. D. Wagman, W. H. Evans, V. B. Parker, R. H. Schumm, I. Halow, S. M. Bailey, K. L. Churney, and R. L. Nuttall, *J. Phys. Chem. Ref. Data* **18**, 1807 (1989).
- <sup>47</sup>D. Zhuang, J. Edgar, B. Strojek, J. Chaudhuri, and Z. Rek, *J. Cryst. Growth* **262**, 89 (2004).